# Why molecules move along a temperature gradient

**Stefan Duhr and Dieter Braun***

Chair for Applied Physics, Ludwig Maximilians Universität, Amalienstrasse 54, 80799 Munich, Germany

Edited by Leo P. Kadanoff, University of Chicago, Chicago, IL, and approved October 12, 2006 (received for review May 26, 2006)

**Molecules drift along temperature gradients, an effect called thermophoresis, the Soret effect, or thermodiffusion. In liquids, its theoretical foundation is the subject of a long-standing debate. By using an all-optical microfluidic fluorescence method, we present experimental results for DNA and polystyrene beads over a large range of particle sizes, salt concentrations, and temperatures. The data support a unifying theory based on solvation entropy. Stated in simple terms, the Soret coefficient is given by the negative solvation entropy, divided by *kT*. The theory predicts the thermodiffusion of polystyrene beads and DNA without any free parameters. We assume a local thermodynamic equilibrium of the solvent molecules around the molecule. This assumption is fulfilled for moderate temperature gradients below a fluctuation criterion. For both DNA and polystyrene beads, thermophoretic motion changes sign at lower temperatures. This thermophilicity toward lower temperatures is attributed to an increasing positive entropy of hydration, whereas the generally dominating thermophobicity is explained by the negative entropy of ionic shielding. The understanding of thermodiffusion sets the stage for detailed probing of solvation properties of colloids and biomolecules. For example, we successfully determine the effective charge of DNA and beads over a size range that is not accessible with electrophoresis.**

DNA | fluorescence | microfluidic | Soret | thermodiffusion

Thermodiffusion has been known for a long time (1), but its theoretical explanation for molecules in liquids is still under debate. The search for a theoretical understanding is motivated by the fact that thermodiffusion in water might lead to powerful all-optical screening methods for biomolecules and colloids. Equally well, thermodiffusion handles and moves molecules all-optically and therefore can complement well established methods: for example, electrophoresis or optical tweezers. For the latter, forces of optical tweezers scale with particle volume and limit this method to particles of only >500 nm. Electrophoresis does not suffer from force limitations but is difficult to miniaturize because of electrochemical reactions at the electrodes.

On the other hand, thermodiffusion allows the microscale manipulation of small particles and molecules. For example, 1,000-bp DNA can be patterned arbitrarily in bulk water (Fig. 1). The temperature pattern "DNA," heated by 2 K, was written into a water film with an infrared laser scanning microscope. The concentration of 1,000-bp DNA was imaged by using a fluorescent DNA tag. In an overall cooled chamber at 3°C, DNA accumulates toward the heated letters "DNA" (negative Soret effect), whereas at room temperature DNA is thermophobic (positive Soret effect) as seen by the dark letters.

In the past, the apparent complexity of thermodiffusion prevented a full theoretical description. As seen for DNA in Fig. 1, molecules characteristically deplete from regions with an increased temperature, but they can also show the inverted effect and accumulate (2, 3). Moreover, the size scaling of thermodiffusion recorded by thermal field flow fractionation showed fractional power laws with a variety of exponents that are hard to interpret (4, 5). The latter effect might be resolved by revealing nonlinear thermophoretic drift for the strong thermal gradients used in thermal field flow fractionation (our unpublished observations).

A variety of methods were used to measure thermodiffusion, mostly in the nonaqueous regime, ranging from beam deflection (2, 3, 6), holographic scattering (7–9), electrical heating (10), to thermal lensing (11). Recently we have developed a fluorescence microfluidic imaging technique (12, 13) that allows the measurement of thermodiffusion over a wide molecule size range without artifacts induced by thermal convection. Highly diluted suspensions can be measured; therefore, particle–particle interactions do not have an influence. We only apply moderate temperature gradients. In the following study, we used this method to confirm a straightforward theoretical explanation of thermodiffusion.

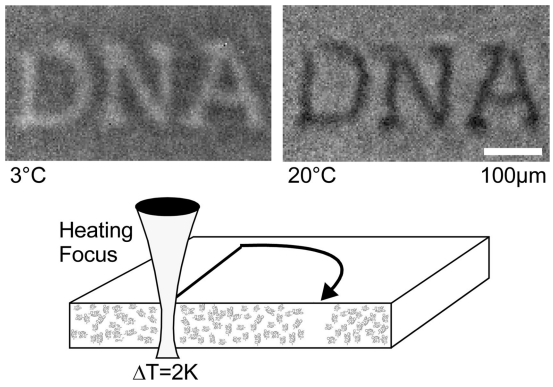


**Fig. 1.** Thermodiffusion manipulates the DNA concentration by small temperature differences within the bulk solution. A thin water film is heated by 2 K along the letters "DNA" with an infrared laser. For a cooled chamber at 3°C, fluorescently tagged DNA accumulates at the warm letters. However, at room temperature, DNA moves into the cold, showing reduced fluorescence. The chamber is 60 $\mu$m thin, containing 50 nM DNA in 1 mM Tris buffer. Every 50th base pair is labeled with TOTO-1 (for details, see supporting information).

## Theoretical Approach

For diluted concentrations, it is generally assumed (14) that the thermodiffusive drift velocity $\vec{v}$ depends linearly on the temperature gradient $\nabla T$ with a proportionality constant which equals the thermodiffusion coefficient $D_T$: $\vec{v} = -D_T \nabla T$. In steady state, thermodiffusion is balanced by ordinary diffusion. Constant diffusion and thermodiffusion coefficients both lead to an exponential depletion law (15) $c/c_0 = \exp[-(D_T/D)(T - T_0)]$, with the concentration $c$ depending on the temperature difference $T - T_0$ only. The concentration $c$ is normalized by the boundary condition of the concentration $c_0$ with temperature $T_0$. The Soret coefficient is defined as ratio $S_T = D_T/D$, which determines the magnitude of thermodiffusion in the steady state. Although the above exponential distribution could motivate an approach based on Boltzmann equilibrium statistics, it is commonly argued that thermodiffusion without exception is a local nonequilibrium effect that requires fluid dynamics, force fields, or particle–solvent potentials (16–20). However, in a previous paper (15), we demonstrated that for moderate temperature

Author contributions: D.B. designed research; S.D. and D.B. performed research; S.D. and D.B. analyzed data; and S.D. and D.B. wrote the paper.

The authors declare no conflict of interest.

*To whom correspondence should be addressed. E-mail: dieter.braun@lmu.de.





www.pnas.org/cgi/doi/10.1073/pnas.0603873103

gradients the thermal fluctuations of the particle are the basis for a local equilibrium. This allows the description of the thermodiffusive steady state by a succession of local Boltzmann laws, yielding $c/c_0 = \exp[-(G(T) - G(T_0))/kT]$, with $G$ being the Gibbs-free enthalpy of the single particle–solvent system. Such an approach is valid only if the temperature gradient $\nabla T$ is below a threshold $\nabla T < (aS_T)^{-1}$, which is given by the particle fluctuations with the hydrodynamic radius $a$ and Soret coefficient $S_T$, as shown recently (15). In the present study, temperature gradients below this limit were used so that thermodiffusion is measured at local thermodynamic equilibrium conditions.

Local thermodynamic equilibrium allows the derivation of a thermodynamic foundation of the Soret coefficient. The local Boltzmann distribution relates small concentration changes $\delta c$ with small Gibbs-free energy differences: $\delta c/c = -\delta G/kT$. We equate this relation with a locally linearized thermodiffusion steady state given by $\delta c/c = -S_T \delta T$ and thus find the Soret coefficient by the temperature derivative of $G$:

$$S_T = D_T/D = (kT)^{-1} \times \partial G/\partial T. \qquad [1]$$

Whereas the above relation is sufficient for the following derivation, it can be generalized by locally applying the thermodynamic relation $dG = -SdT + Vdp + \mu dN$. For single particles at a constant pressure we find that the Soret coefficient equals the negative entropy of the particle–solvent system $S$ according to $S_T = -S/kT$. This relation is not surprising given that the entropy is by definition related with the temperature derivative of the free enthalpy.

The above general energetic treatment is inherent in previously described approaches based on local equilibrium (14, 21, 22), including the successful interpretation of thermoelectric voltages of diluted electrolytes (23, 24), which are described by energies of transfer. Recently, the nonequilibrium approach by Ruckenstein (25) was applied to colloids (26) with the characteristic length $l$ assigned to the Debye length $\lambda_{DH}$. If instead one would assign the characteristic length according to $l = 2a/3$ with the particle radius $a$, the Ruckenstein approach would actually confirm the above local equilibrium relation (1) for the Soret coefficient. Measurements on SDS micelles (26) appeared to confirm this nonequilibrium approach, but for the chosen particles the competing parameter choices $l = 2a/3$ and $\ell = \lambda_{DH}$ yielded comparable values. Thus, the experiments could not distinguish between the competing theories.

We will use the above local equilibrium relations to derive the Soret coefficient for particles larger than the Debye length in aqueous solutions and put the results to rigorous experimental tests. Two contributions dominate the particle entropy $S$ in water (Fig. 2*a*): the entropy of ionic shielding (Fig. 2a *Left*) and the temperature-sensitive entropy of water hydration (Fig. 2*a Right*). The contribution from the entropy of ionic shielding is calculated with the temperature derivative of the Gibbs-free enthalpy (26, 27) $G_{ionic} = Q_{eff}^2 \lambda_{DH}/[2A\varepsilon\varepsilon_0]$ with the effective charge $Q_{eff}$ and particle surface $A$. Alternatively, this enthalpy can be interpreted as an electrical field energy $G_{ionic} = Q_{eff}^2/[2C]$ in the ionic shielding capacitor $C$. We neglect the particle–particle interactions because the fluorescence approach allows the measurement of highly diluted systems. To obtain the Soret coefficient, temperature derivatives consider the Debye length $\lambda_{DH}(T) = \sqrt{\varepsilon(T)\varepsilon_0 kT/(2e^2 c_S)}$ and the dielectric constant $\varepsilon(T)$. Both temperature derivatives give rise to a factor $\beta = 1 - (T/\varepsilon)\partial\varepsilon/\partial T$. The effective charge $Q_{eff}$ is largely temperature-insensitive, which was confirmed by electrophoresis independently (28). Such a dependence would be unexpected because the strongly adsorbed ions dominate the value of the effective charge. Experimentally, we deal with colloids exhibiting flat surfaces, i.e., the particle radius is larger than $\lambda_{DH}$. In this case, charge renormalization does not play a role and we can introduce an effective surface charge density $\sigma_{eff} = Q_{eff}/A$ per molecule area $A$. From the temperature derivation according to Eq. **1**, the ionic contribution to the Soret coefficient is $S_T^{(ionic)} = (A\beta\sigma_{eff}^2\lambda_{DH})/(4\varepsilon\varepsilon_0 kT^2)$. A similar relation was derived for charged micelles recently (22), although without considering the temperature dependence of the dielectric coefficient $\varepsilon$. Next, the contribution to the Soret coefficient from the hydration entropy of water can be directly inferred from the particle-area-specific hydration entropy $s_{hyd} = S_{hyd}/A$, namely $S_T^{(hyd)} = -As_{hyd}(T)/kT$. Finally, the contribution from the Brownian motion is derived as $S_T = 1/T$ by inserting the kinetic energy of the particle $G = kT$ into Eq. **1**. However, this contribution is very small ($S_T = 0.0034$/K) and can be neglected for the molecules under consideration. The contributions from ionic shielding and hydration entropy add up to

$$S_T = \frac{A}{kT}\left( -s_{hyd} + \frac{\beta\sigma_{eff}^2}{4\varepsilon\varepsilon_0 T} \times \lambda_{DH} \right). \qquad [2]$$

The Soret coefficient $S_T$ scales linearly with particle surface $A$ and Debye length $\lambda_{DH}$. We tested Eq. **2** by measuring $S_T$ versus salt concentration, temperature, and molecule size. In all cases, thermodiffusion is quantitatively predicted without any free parameters. We used fluorescence single-particle tracking to follow carboxyl-modified polystyrene beads (catalog no. F-8888, Molecular Probes, Eugene, OR) with diameters of 1.1 and 0.5 at 25 aM dialyzed into 0.5 mM Tris·HCl at pH 7.6. Thermodiffusion of particles $\leq 0.2$ $\mu$m is measured by the fluorescence decrease that reflects the bulk depletion of the particles (12). The chamber thickness of 20 $\mu$m damped the thermal convection to negligible speeds (15). The experimental design also excludes thermal lensing and optical trapping (15). Debye lengths $\lambda_{DH}$ were titrated with KCl (see the supporting information, which is published on the PNAS web site).

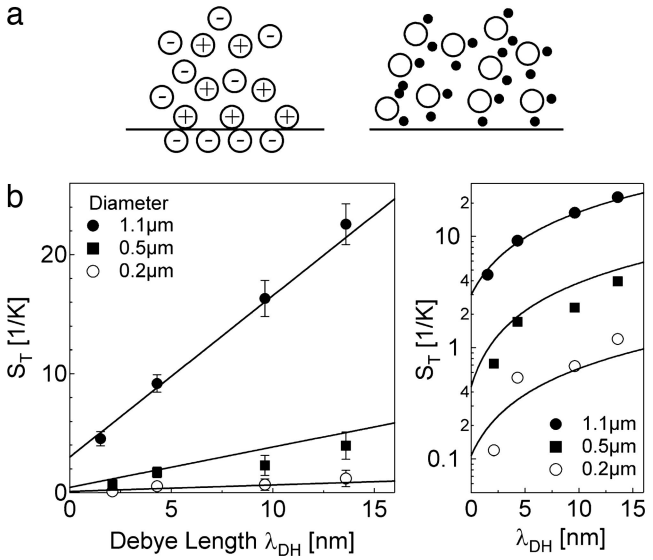


**Fig. 2.** Salt dependence. (*a*) Thermodiffusion in water is dominated by ionic shielding (*Left*) and water hydration (*Right*). (*b*) Soret coefficient $S_T$ versus Debye length for carboxyl-modified polystyrene beads of diameter 1.1, 0.5, and 0.2 $\mu$m. Linear plot (*Left*) and logarithmic plot (*Right*). The Soret coefficients are described by Eq. **2** with an effective surface charge of $\sigma_{eff} = 4{,}500$ e/$\mu$m$^2$ known from electrophoresis. The intercept $S_T(\lambda_{DH} = 0)$ is fitted with a hydration entropy per particle surface of $s_{hyd} = -1{,}400$ J/(mol·K·$\mu$m$^2$).

**Salt Dependence.** Fig. 2*b* shows the Soret coefficients of polystyrene beads with different sizes versus $\lambda_{DH}$. The Soret coefficients

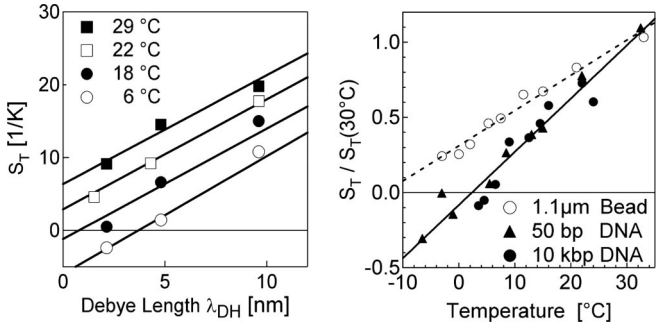


**Fig. 3.** Temperature dependence. (*a*) The temperature dependence is dominated by the linear change in the hydration entropy $S_{hyd}$. It shifts the salt-dependent thermodiffusion $S_T(\lambda_{DH})$ to lower values. The particle size is 1.1 $\mu$m. (*b*) The Soret coefficient $S_T$ increases linearly with the temperature as expected for a hydration entropy $S_{hyd}(T)$. It depends on the molecule species, not its size, as seen from the rescaled Soret coefficients for DNA with different lengths.

scale linearly with a small intercept at $\lambda_{DH} = 0$ and confirm the $\lambda_{DH}$-dependence of Eq. 2. For smaller-diameter beads, the Soret coefficients scale with the particle surface area $A$ (Fig. 2), as expected from Eq. **2**. To check whether Eq. **2** also quantitatively explains the measured Soret coefficients, we inferred the effective charge of the beads by electrophoresis (see supporting materials). By using 40-nm beads with identical carboxyl surface modifications at $\lambda_{DH} = 9.6$ nm, we fluorescently observed free-flow electrophoresis and corrected for electroosmosis, finding an effective surface charge density of $\sigma_{eff} = 4{,}500 \pm 2{,}000$ e/$\mu$m$^2$. This value is virtually independent from the used salt concentrations (28). With this inferred effective charge, Eq. **2** fits the Soret coefficient for various bead sizes and salt concentrations well (Fig. 2*b*, solid lines).

The intercept $S_T(\lambda_{DH} = 0)$, where ionic contributions are zero, also scales with particle surface and is described by a hydration entropy per particle surface of $s_{hyd} = -1{,}400$ J/(mol·K·$\mu$m$^2$). The value matches the literature values for similar surfaces reasonably well (29–31). For example, dansyl-alanine, a molecule with surface groups comparable with polystyrene beads, was measured to have a hydration entropy (29) of $-0.13$ J/(mol·K) at a comparable temperature. Linear scaling with its surface area by using a radius of $a = 2$ nm results in a value of $s_{hyd} = -2{,}500$ J/(mol·K·$\mu$m$^2$), in qualitative agreement with our result. The hydration entropy is a highly informative molecule parameter that is notoriously difficult to measure, yielding an interesting application for thermodiffusion.

**Temperature Dependence.** Hydration entropies $S_{hyd}$ in water are known to increase linearly with decreasing temperatures (29–31). Because the slope of the ionic contribution of $S_T$ versus $\lambda_{DH}$ is with high-precision temperature insensitive for water [$\beta(T)/(\varepsilon T^2) \cong$ const], only the intercept is expected to decrease as the overall temperature of the chamber is reduced. This is indeed the case, as seen from the temperature dependence of beads with diameters of 1.1 $\mu$m ($T = 6$–29°C) (Fig. 3*a*). We infer from the intercept $S_T(\lambda_{DH} = 0)$ that the hydration entropy changes sign at ≈20°C. As seen for DNA in Fig. 1, hydration entropy can dominate thermodiffusion at low temperatures and move molecules toward the heat ($D_T < 0$).

The properties of hydration entropy lead to a linear increase of $S_T$ over temperatures at a fixed salt concentration as measured for 1.1-$\mu$m beads and DNA (Fig. 3*b*). We normalized $S_T$ by dividing by $S_T$(30°C) to compensate for molecule surface area. The slopes of $S_T$ over temperature differ between beads and DNA. However the slope does not differ between DNA of different size (50 bp versus 10,000 bp). Based on Eq. **2**, this is to be expected because the temperature dependence of the hydration entropy depends only on the type of surface of the molecule, not its size. We measured the diffusion coefficients of the DNA species at the respective temperature independently. Within experimental error, changes in the diffusion coefficient $D$ match with the change of the water viscosity without the need to assume conformational changes of DNA over the temperature range. Please note that the change of the sign of the DNA Soret coefficient is situated near the point of maximal water density only by chance. There, the two entropic contributions balance. For polystyrene beads at $\lambda_{DH} = 2$ nm for example, the sign change is observed at 15°C (Fig. 3*a*). An increased Soret coefficient over temperature was reported for aqueous solutions before (3), however with a distinct nonlinearity that we attribute to remnant particle–particle interactions.

**Size Dependence of the Beads.** The Soret coefficient was measured for carboxyl-modified polystyrene beads in diameters ranging from 20 nm to 2 $\mu$m. Beads with diameters of 0.2, 0.1, 0.04, and 0.02 $\mu$m were diluted to concentrations of 10 pM, 15 pM, 250 pM, and 2 nM, and their bulk fluorescence was imaged over time to derive $D_T$ and $D$ (12, 15) from the depletion and subsequent back-diffusion. Larger beads with diameters of 1.9, 1.1, and 0.5 $\mu$m were diluted to concentrations of 3.3 aM, 25 aM, and 0.2 pM and measured with single-particle tracking. The solutions were buffered in 1 mM Tris (pH 7.6) with $\lambda_{DH} = 9.6$ nm. In all cases, interactions between particles can be excluded. Care was taken to keep the temperature gradient in the local equilibrium regime.

We find that the Soret coefficient scales with particle surface over four orders of magnitude (Fig. 4*a*). The data are described well with Eq. **2** with an effective surface charge density of $\sigma_{eff} = 4{,}500$ e/$\mu$m$^2$ and neglected hydration entropy contribution. The 5-fold too-low prediction for the smallest particle (20 nm in diameter) can be explained by charge renormalization because its radius is smaller than $\lambda_{DH}$.

The diffusion coefficient $D$ for spheres is given by the Einstein relation and scales inversely with radius $D \propto 1/a$. Inserting Eq. **2** into $S_T = D_T/D$, the thermodiffusion coefficient $D_T$ is expected to scale with particle radius $a$. This is experimentally confirmed over two orders of magnitude (Fig. 4*b*). These findings contradict several theoretical studies claiming that $D_T$ should be independent of particle size (16–20, 26), based on ambiguous experimental results from thermal field flow fractionation (4) that were probably biased by nonlinear thermodiffusion in large thermal gradients (15).

**Size Dependence of DNA.** Whereas polystyrene beads share a very narrow size distribution as a common feature with DNA molecules, beads are a much less complicated model system. Beads are rigid spheres that interact with the solvent only at its surface. In addition, the charges reside on the surface, where the screening takes place. Thus, the finding that thermodiffusion of flexible and homogeneously charged DNA is described equally well with Eq. **2** is not readily expected and quite interesting (Fig. 4 *c* and *d*).

We measured DNA with sizes of 50–48,502 bp in 1 mM Tris buffer ($\lambda_{DH} = 9.6$ nm) at low molecule concentrations between 1 $\mu$M (50 bp) and 1 nM (48,502 bp). Only every 50th base pair was stained with the TOTO-1 fluorescent dye. The diffusion coefficient was measured by back-diffusion after the laser was turned off and depends on the length $L$ of the DNA in a nontrivial way. The data are well fitted with a hydrodynamic radius scaling $a \propto L^{0.75}$. This scaling represents an effective average over two DNA length regimes. For DNA molecules longer than ≈1,000 bp, a scaling of 0.6 is found (32), whereas shorter DNA scales with an exponent of ≈1 (see the supporting information).

We can describe the measured Soret coefficient over three

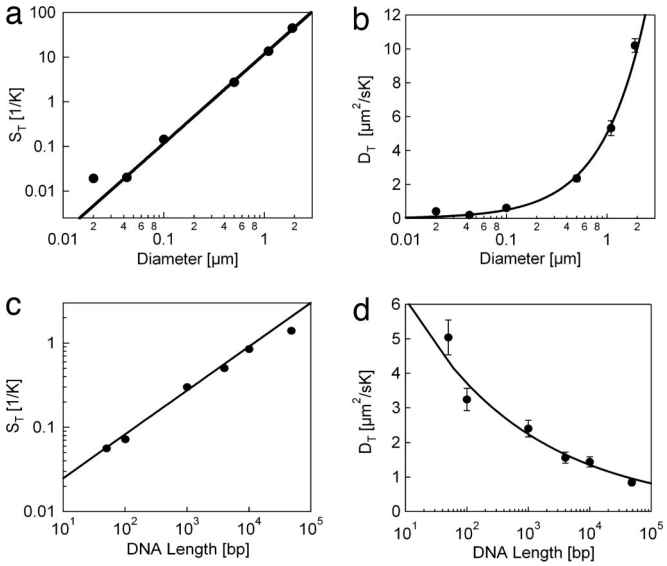


**Fig. 4.** Size dependence. (*a*) For polystyrene beads, the Soret coefficient scales with the particle surface over four orders of magnitude. Measurements are described by Eq. **2** with an effective surface charge density of $\sigma_{eff}$ = 4,500 e/$\mu$m$^2$ (2) and negligible hydration entropy. The deviation for the bead with a diameter of 20 nm can be understood from an increased effective charge due to the onset of charge normalization for $a \leq \lambda_{DH}$. (*b*) Accordingly, the thermodiffusion coefficient $D_T$ scales linearly with bead diameter. (*c*) The Soret coefficient of DNA scales according to $S_T \propto \sqrt{L}$, with the length $L$ of the DNA based on Eq. **2** with an effective charge per base pair of 0.12 e. (*d*) Thermodiffusion coefficient $D_T$ decreases over DNA length with $D_T \propto L^{-0.25}$, caused by the scaling of diffusion coefficient $D \propto L^{-0.75}$.

orders of magnitude of DNA lengths with Eq. **2** if we assume that effective charge of the DNA is shielded at the surface of a sphere with the hydrodynamic radius $a$. Because of the low salt concentration ($\lambda_{DH}$ = 9.6 nm), such globular shielding is reasonable. Not only is the experimentally observed scaling of the Soret coefficient with the square root of its length correctly predicted based on Eq. **2** ($S_T \propto Q_{eff}^2/a^2 \propto L^2/L^{1.5} \propto L^{0.5}$), but the Soret coefficient also is fully described in a quantitative manner (Fig. 4*c*, solid line), with an effective charge of 0.12 e per base, matching well with literature values (33) ranging from 0.05 e/bp to 0.3 e/bp.

As shown in Fig. 4*d*, the thermodiffusion coefficient for DNA drops with DNA length according to $D_T = DS_T \propto Q_{eff}^2/a^3 \propto L^2/L^{2.25} \propto L^{-0.25}$. Thus, shorter DNA actually drifts faster in a temperature gradient than longer DNA. It is important to point out that this finding is in no way contradictory to experimental findings of a constant $D_T$ over polymer length in nonaqueous settings (8). According to Eq. **1**, the thermodynamic relevant parameter is the Soret coefficient, which is determined by the solvation energetics. The argument (19) that polymers have to decouple into monomers to show a constant $D_T$ merely becomes the special case where the solvation energetics determine both $S_T$ and $D$ with equal but inverted size scaling. In accordance with our local energetic equilibrium argument, $S_T$ and not $D_T$ dominates thermodiffusion also for nonaqueous polymers near a glass transition (8). Here, $S_T$ is constant, whereas $D_T$ and $D$ scale according to an increased friction. However, for a system of DNA in solution, for which long-ranging shielding couples the monomers, a constant $D_T$ over polymer length cannot be assumed *a priori* (Fig. 4*d*).

**Effective Charge.** The effective charge $Q_{eff}$ is a highly relevant parameter for colloid science, biology, and biotechnology. So far it only could be inferred from electrophoresis, restricted to

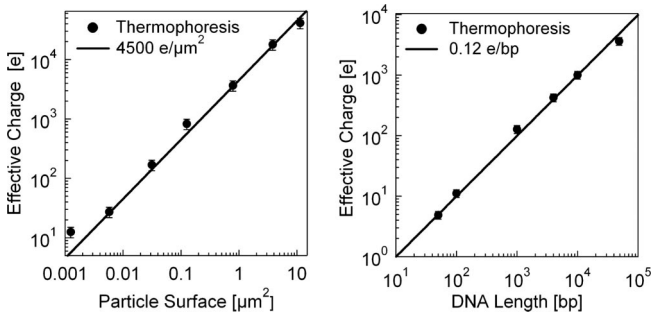


**Fig. 5.** Effective charge from thermodiffusion. Effective charge is inferred from thermodiffusion using Eq. **3**. Polystyrene beads (20–2,000 nm) (*a*) and DNA (50–50,000 bp) (*b*) were measured over a large size range, which is impossible with electrophoresis. As expected, the effective charge of the beads scales with particle surface and linearly with the length of DNA.

particles smaller than the Debye length ($a \leq 3\lambda_{DH}$) (34). Unfortunately, many colloids are outside this regime. As shown before, a similar size restriction does not hold for thermodiffusion. In many cases, the hydration entropy $s_{hyd}$ contributes <15% (Fig. 2) and can be neglected at moderate salt levels. Thus, we can invert Eq. **2** to obtain the effective charge $Q_{eff}$ for spherical molecules from

$$Q_{eff} = \frac{2T^2}{3\eta D}\sqrt{\frac{\varepsilon\varepsilon_0 k^3 S_T}{\beta\pi\lambda_{DH}}}. \quad [3]$$

The effective charge derived from thermodiffusion measurements of polystyrene beads and DNA is plotted in Fig. 5 over several orders of magnitude in size. The effective charge of beads scales linearly with particle surface, with a slope confirming the effective surface charge density of $\sigma_{eff}$ = 4,500 e/$\mu$m$^2$, which was inferred from electrophoresis only for small particles. Average deviations from linear scaling are <8% (Fig. 5*a*). The effective charge inferred from thermodiffusion measurements of DNA using Eq. **3** scales linearly with DNA length with an effective charge of 0.12 e/bp. The length scaling is confirmed over four orders of magnitude with an average error of 12% (Fig. 5*b*). Thus, thermodiffusion can be used to infer the effective charge with low errors for a wide range of particle sizes. This is even more interesting for biomolecule characterization because measurements of thermodiffusion can be performed all-optically in picoliter volumes.

## Conclusion

We describe thermodiffusion, the molecule drift along temperature gradients, in liquids with a general, microscopic theory. Applied to aqueous solutions, this theory predicts thermodiffusion of DNA and polystyrene beads with an average accuracy of 20%. We experimentally validate major parameter dependencies of the theory: linearity against screening length $\lambda_{DH}$ and molecule hydrodynamic area $A$, quadratic dependence on effective charge, and linearity against temperature. Measurements of thermodiffusion can be miniaturized to the micrometer scale with the all-optical fluorescence technique and permit microscopic temperature differences to manipulate molecules based on their surface properties (Fig. 1). The theoretical description allows the extraction of solvation entropy and the effective charge of molecules and particles over a wide size range.

## Materials and Methods

**Infrared Temperature Control.** The temperature gradients used to induce thermodiffusive motions were created by aqueous absorption of an infrared laser (Furukawa Electric, Tokyo, Japan) at a wavelength of 1,480 nm and 25 mW of power. Water strongly

absorbs at this wavelength with an attenuation length of $\kappa = 320$ $\mu$m. The laser beam was moderately focused with a lens of 8-mm focal distance. Typically, the temperature in the solution was raised by 1–2 K in the beam center with a $1/e^2$ diameter of 25 $\mu$m, measured with the temperature-dependent fluorescence signal of the dye 2′,7′-bis(carboxyethyl)-5(6)-carboxyfluorescein (12). Thin chamber heights of 10–20 $\mu$m and moderate focusing removed possible artifacts from optical trapping, thermal lensing, and thermal convection (12). For temperature-dependent measurements, both the objective and the microfluidic chip were tempered with a thermal bath. Imaging was provided from an AxioTech Vario fluorescence microscope (Zeiss, Oberkochen, Germany), illuminated with a high-power light-emitting diode (Luxeon, Calgary, Canada), and recorded with the CCD camera SensiCam QE (PCO, Kelheim, Germany).

**Molecules.** Highly monodisperse and protein-free DNA of 50, 100, 1,000, 4,000, 10,000, and 48,502 bp (Fast Ruler fragments and λ-DNA; Fermentas, St. Leon-Rot, Germany) were diluted to 50 $\mu$M base pair concentration, i.e., the molecule concentration was between 1 $\mu$M (50 bp) and 1 nM (48,502 bp). DNA was fluorescently labeled by the intercalating TOTO-1 fluorescent dye (Molecular Probes) with a low dye/base pair ratio of 1:50. Carboxyl-modified polystyrene beads with diameters of 2, 1, 0.5, 0.2, 0.1, 0.04, and 0.02 $\mu$m (catalog nos. F-8888, F-8823, F-8827, F-8888, F-8795, F-8823, and F-8827; Molecular Probes) were dialyzed (Eluta Tube mini; Fermentas) in distilled water and diluted in 1 mM Tris (pH 7.6) to concentrations between 3.3 aM (2 $\mu$m) and 2 nM (0.02 $\mu$m).

**Concentration Imaging Over Time.** Either the method of concentration imaging (12) or single-particle tracking was used to measure thermodiffusion at low concentrations, namely $<0.03$ g/liter for DNA and $10^{-5}$ g/liter for beads. At higher concentrations, we found profound changes of thermodiffusion coefficients. DNA and polystyrene beads of $<0.5$ $\mu$m in diameter were imaged over time (12) by bright-field fluorescence with a $\times 40$ oil-immersion objective. Concentrations inferred after correcting for bleaching, inhomogeneous illumination, and temperature-dependent fluorescence (12) were fitted with a finite element theory. The model captures all details of both thermodiffusive depletion and back-diffusion to measure $D_T$ and $D$ independently (see supporting information). Measurements were performed in microfluidic chips 10 $\mu$m in height with polydimethylsiloxane on both sides.

**Single-Particle Tracking.** Polystyrene particles of $>0.5$ $\mu$m in diameter were measured by single-particle tracking due to the slow equilibration time and risk that steady-state depletion is disturbed by thermal convection. The thermodiffusive drift was imaged with a $\times 32$ air objective at 4 Hz at an initial stage of depletion in a 20-$\mu$m-thick chamber. Averaging over the $z$ position of the particles removed effects from thermal convection. The drift velocity versus temperature gradient of 400 tracks were linearly fitted by $v = -D_T \nabla T$ to infer $D_T$. The diffusion coefficients $D$ of the particles were evaluated based on their squared displacement, matching within 10% the Einstein relationship.

We thank Klaus Stierstadt, Jan Dhont, and Werner Köhler for discussions and Julia Morfill and Veronica Egger for comments on the manuscript. Our Emmy-Noether Group is funded by the Deutsche Forschungsgemeinschaft and hosted by Hermann Gaub.

1. Ludwig C (1856) *Sitzungber Bayer Akad Wiss Wien Math-Naturwiss Kl* 20:539.
2. Giglio M, Vendramini A (1977) *Phys Rev Lett* 38:26–30.
3. Iacopini S, Piazza R (2003) *Europhys Lett* 63:247–253.
4. Jeon SJ, Schimpf ME, Nyborg A (1997) *Anal Chem* 69:3442–3450.
5. Shiundu PM, Liu G, Giddings JC (1995) *Anal Chem* 67:2705–2713.
6. Piazza R, Guarino A (2002) *Phys Rev Lett* 88:208302.
7. de Gans BJ, Kita R, Müller B, Wiegand S (2003) *J Chem Phys* 118:8073–8081.
8. Rauch J, Köhler W (2002) *Phys Rev Lett* 88:185901.
9. Wiegand S, Köhler W (2002) in *Thermal Nonequilibrium Phenomena in Fluid Mixtures* (Springer, Berlin), p 189.
10. Putnam SA, Cahill DG (2005) *Langmuir* 21:5317–5323.
11. Rusconi R, Isa L, Piazza R (2004) *J Opt Soc Am B* 21:605–616.
12. Duhr S, Arduini S, Braun D (2004) *Eur Phys J E* 15:277–286.
13. Braun D, Libchaber A (2002) *Phys Rev Lett* 89:188103.
14. de Groot SR, Mazur P (1969) *Nonequilibrium Thermodynamics* (North–Holland, Amsterdam).
15. Duhr S, Braun D (2006) *Phys Rev Lett* 96:168301.
16. Emery AH, Jr, Drickamer HG (1955) *J Chem Phys* 23:2252–2257.
17. Ham J (1960) *J Appl Phys* 31:1853–1858.
18. Morozov KI (1999) *J Exp Theor Phys* 88:944–946.
19. Schimpf ME, Semenov SN (2000) *J Phys Chem B* 104:9935–9942.
20. Voit A, Krekhov A, Enge W, Kramer L, Köhler W (2005) *Phys Rev Lett* 92:214501.
21. Dhont JKG (2004) *J Chem Phys* 120:1632–1641.
22. Fayolle S, Bickel T, Le Boiteux S, Würger A (2005) *Phys Rev Lett* 95:20830.
23. Agar JN, Turner JCR (1960) *Proc R Soc London Ser A* 255:307–329.
24. Snowdon PN, Turner JCR (1960) *Trans Faraday Soc* 56:1409–1418.
25. Ruckenstein E (1981) *J Colloid Interface Sci* 83:77–85.
26. Piazza R, Guarino A (2002) *Phys Rev Lett* 88:208302.
27. Israelachvili J (1992) *Intermolecular and Surface Forces* (Academic, New York), 2nd Ed.
28. Lin W, Galletto P, Borkovec M (2004) *Langmuir* 20:7465–7473.
29. Haidacher D, Vailaya A, Horváth C (1996) *Proc Natl Acad Sci USA* 93:2290–2295.
30. Southall NT, Dill KA, Haymet ADJ (2002) *J Phys Chem B* 106:521–533.
31. Kronberg B, Costas M, Silveston R (1995) *Pure Appl Chem* 67:897–902.
32. Pluen A, Netti PA, Jain RK, Berk DA (1999) *Biophys J* 77:542–552.
33. Smith SB, Bendich AJ (1990) *Biopolymers* 29:1167–1173.
34. O'Brien RW, White LR (1978) *J Chem Soc Faraday Trans 2* 74:1607–1626.